A high aspect ratio membrane reactor for liquid-liquid extraction

A high aspect ratio membrane reactor for liquid-liquid extraction

Jonas Hereijgers,[1,2] Manly Callewaert, [1,3] Xinjian Lin,[1] Harry Verelst,[1] Tom Breugelmans,[2]

Heidi Ottevaere,[3] Gert Desmet[1] and Wim De Malsche[1*]

[1]*Department of Chemical Engineering, Vrije Universiteit Brussel, Pleinlaan 2, 1050 Brussel, Belgium*
[2]*Department of Applied Engineering & Technology - Chemistry, Artesis University College, 2000 Antwerpen, Belgium*
[3]*B-PHOT, Department of Applied Physics, Vrije Universiteit Brussel, Pleinlaan 2, 1050 Brussel, Belgium*

*Corresponding author: tel. (+) 32/ 2.629.33.18, fax (+) 32/ 2.629.32.48, e-mail:

wdemalsc@vub.ac.be

Abstract

In the present study, a high aspect ratio membrane reactor was evaluated in terms of extraction efficiency in co- and countercurrent flow using 2 different membrane types (Teflon® and polycarbonate). Using the parallel plate Poiseuille expression to approximate the flow profile in flat rectangular channels with high aspect ratios an analytical solution was established to describe the concentration profiles in the microcontactor for non-miscible mixtures, which was numerically and experimentally validated. Fast and uniform mass transfer could be enabled by providing ordered spacers of 100 and 200 µm in the reactor substrate. With the flow rates in this optimization being limited by the Laplace pressure of the membrane, a pressure driven alternative mimicked by adapting the flow rates inversely to the liquid viscosity ratios is analyzed and experimentally validated for co-current mode. Using the device in co-current mode, the system has the potential to serve as a fast screening tool to determine partition coefficients requiring 5-15 min per combination only. It was furthermore analyzed how the channel depth should be adapted when aiming to maximize the extracted mass. Similarly, also the optimal depth to achieve a preset concentration specification was analyzed.

Keywords

liquid-liquid extraction, extraction kinetics, membrane microcontactor, microreactor, solvent screening

Symbol list

C	Concentration analyte	(mol/m³)
D	Diffusion coefficient	(m²/s)
E	Extraction efficiency	(\)
H	Partition coefficient ($C_{s,\,eq}/C_{f,\,eq}$)	(\)
h	Channel depth	(m)
J	Flux	(mol/m² s)

K	Overall mass transfer coefficient	(m/s)
k	Mass transfer coefficient	(m/s)
L	Length of the microcontactor	(m)
N	Number of theoretical stages	(\)
Q	Flow rate	(m^3/s)
Sh	Sherwood number	(\)
u	Velocity	(m/s)
w	Width of the microcontactor channel	(m)
X	Fraction of the partition coefficient	(\)
x	Axial length	(m)
z	Lateral length	(m)

Greek symbols

δ	Thickness of the membrane	(m)
ε	Porosity of the membrane	(\)
τ	Tortuosity	(\)

Subscript

0	Axial position in the microcontactor at x = 0
eff	Effective
f	Feed
L	Axial position in the microcontactor at x = L
m	Membrane
max	Maximum
s	Extraction solvent

1. Introduction

Membrane processes are predominantly used in a wide variety of industrial and medical applications for the separation of cells, colloids, macromolecules, ions, etc. Liquid-liquid extraction is considered a good alternative for separation when distillation fails, but also has a number of fundamental benefits. When dealing with non-volatile phases, nearly equal boiling points inhibit the use of distillation. Also, the use of thermo-labile components is prohibited and the large power consumption becomes more and more relevant [1]. For analytical purposes, liquid-liquid extraction is widely applied as a tool for sample preparation prior to analysis. By reducing the required contact time, different extraction techniques have been developed. Membrane based extraction techniques constitute herein a considerable portion. The membrane serves as an interface stabilizer to avoid a compulsory phase separation step after the extraction.

Hollow fibers have been the traditional format to integrate membranes into channels for decades now, and it is well known that mass transfer characteristics for e.g. multi-phase operations can be improved considerably as compared to traditional approaches [2]. A fundamental limitation of hollow fibers is that the extraction kinetics are adversely affected when aiming at a larger column cross section with a concomitant increase in diffusion distances. A possible approach consists of minimizing the fiber diameter and maximizing the number of hollow fibers in a module. The occurrence of dead zones, backmixing, bypassing and channeling, especially on the shell side, causing irregular mass transfer along the module [3] thereby present however serious drawbacks. The technological ability to decrease diffusive distances by means of different microfabrication approaches has lead to a number of other promising approaches [4, 5].

In supported liquid membrane (SLM) extraction [6, 7] a hydrophobic membrane holds an organic solvent, with the channels oriented at either side of the membrane and filled with aqueous phases at a different pH. Using the appropriate pH values, this approach enables an enormous enrichment for charged basic or acidic analytes [8]. When the analytes render charged after diffusion through the organic phase, it becomes energetically highly unfavorable to pass again to the other aqueous stream. This membrane technique is mostly operated semi-continuously with the acceptor phase held stagnant during the extraction, while the donor phase is pumped at a given flow rate.

A variant of SLM is electromembrane extraction (EME) in which an electric field is applied across the membrane enhancing the extraction kinetics. By placing an electrode in both channels with a DC potential across the membrane, a driving force enabling mass transport beyond Fick’s law is generated, resulting in large extraction efficiencies (70-80%) in micromachined channels with critical dimensions of 50 μm in 5 minutes only. [9, 10] Due to

the high electric resistance of the membrane and the low voltage that is applied, electrolysis can generally be avoided in this operation mode.

A more robust configuration is conceived when the membrane stabilizes the interface by a preferential wetting of one phase. The need to perform a phase separation is hence omitted in this approach. The last two decades there has been an increasing trend to integrate several functions into a single reactor and to intensify chemical processes. The advantages offered by continuous operation at small length scales in closed systems such as reduced reaction volumes and enhanced heat and mass transfer are indeed very appealing [11]. The very controlled formation of droplets enables very sharp droplet size distributions with a concomitant large control on extraction kinetics. When the droplets are large and form adjacent slugs within capillaries or microchannels internal recirculation takes place, resulting in faster internal mass transport and a reduced thickness of the interfacial boundary layer, hence enhancing the extraction kinetics [12]. A disadvantage of droplet-based approaches is that a phase separation after the extraction is required [13], but also that the operation window wherein e.g. slugs are formed (and e.g. not a stratified flow) is limited. Also the size of slugs is affected by the liquid properties, making the kinetics unpredictable when the conditions are varied [14].

A number of approaches have been pursued to stabilize the interface in microreactors. Maruyama et al. [15] carried out liquid-liquid extraction of metal ions in a Pyrex-based microfluidic device containing intermittent partition walls to stabilize an n-heptane-water interface. Treatment of the channel surface with a self-assembled monolayer has also proven to be effective in stabilizing the interface. Hibara et al. [16] demonstrated a tolerated pressure difference of ~600 Pa to maintain a stable interface. Etching grooves provide yet another means to stabilize the interface. Using 5 μm high guide structures in a 20 μm deep channel

Tokeshi et al. [17] was in this way able to stabilize a triple parallel flow of m-xylene , hydrogen chloride and sodium hydroxide solution at flow rates of 0.4 µl/min, 0.2 µ/min and 0.2 µl/min, respectively. The addition of surfactant improves the interface stability, favoring stratified flow over segmented flow [18]. By examining different membranes, Dupuy et al. [19] showed the influence of the surface properties and pore size on to the breakthrough pressure, reaching up to 0.98 bar.

These approaches have in common that two streams are contacted by a vertical interface. This configuration produces a small contact area because microfabrication limitations hinder the achievement of large channel depths. The interface area can however be dramatically increased when a wide and shallow channel is used. An additional advantage of this approach is that commercially available membranes can be easily integrated in the reactor. Even though that sandwiching of membranes between milled reactor substrates is well known in the field of sample preparation for supported liquid membranes [6-8], this approach has been surprisingly hardly implemented for classical two-phase extraction [20]. The ability to use much wider than deep channels has been hardly pursued [19, 21], even though that the use of such high aspect ratio channels is the key to enable reasonable flow rates in this format when aiming at improving mass transfer kinetics [14]. A critical feature in this reactor design is flow distribution at the inlet and outlet in the reactor. Our group has recently proposed a format containing support structures to enable a uniform distribution in wide channels [22], which was recently applied in the frame of sample preparation for HPLC analysis in a drug uptake study [21]. Besides being a valuable tool for efficient extraction when only limited sample is available in biological studies, the format also has the potential to become a crucial tool in the production scheme of pharmaceuticals. When the required time to determine the optimal extraction conditions as well as the necessary sample mass can be reduced and perhaps even automated automatically, such a screening tool would be well received in the

pharmaceutical industry [23]. On the other hand, there is a demand for small extraction units for the early stages in drug development [24].

In the present paper, the kinetics of high aspect ratio channels are modeled and solved analytically. The obtained equations for co- and counterflow operation are subsequently validated by numerical simulation and by experimentally extracting 1-propanol from heptane to water using two different membranes and a set of flow rate and channel depth combinations. The paper concludes with a number of theoretical considerations to guide the reactor design for a number of application demands.

2. Experimental

2.1 Chemicals

n-Heptane and 1-propanol was purchased from Sigma-Aldrich with a purity of 99.9+%. The water used throughout the experiments was prepared in the laboratory (Milli-Q-gradient, Millipore, Bedford, MA, USA).

2.2 Apparatus

The microcontactor consists of two milled (Datron CNC mill) aluminium bodies that are clamped together, sandwiching a Teflon or polycarbonate membrane (Table 1) with respectively hydrophobic and hydrophilic surface properties. The milled channels are 90 mm long from distributor to distributor, the distributor itself is 5 mm long, the channels are 13 mm wide and 100 μm or 200 μm deep. Pillars of 1 mm diameter were defined in the channels to ensure a constant distance between the membrane and the plates. Sealing at the periphery is assured by a compressed Kalrez O-ring (Eriks-Boudain, Antwerp, Belgium). At the inlet and the outlet of the channels a distributor is defined (Fig. 1) to guarantee a uniform flow

distribution. The inlet and outlet consist of a 1 mm drilled cylindrical hole which are connected to a syringe pump (kd Scientific) and a collection vessel with the use of capillaries.

Material	Supplier	Porosity (%)	Thickness (µm)	Average Pore Size (µm)
Teflon	Frisenette Aps	68.0	70	0.10
Polycarbonate	Millipore	13.8	30	0.2

Table 1: Specifications of the examined membranes.

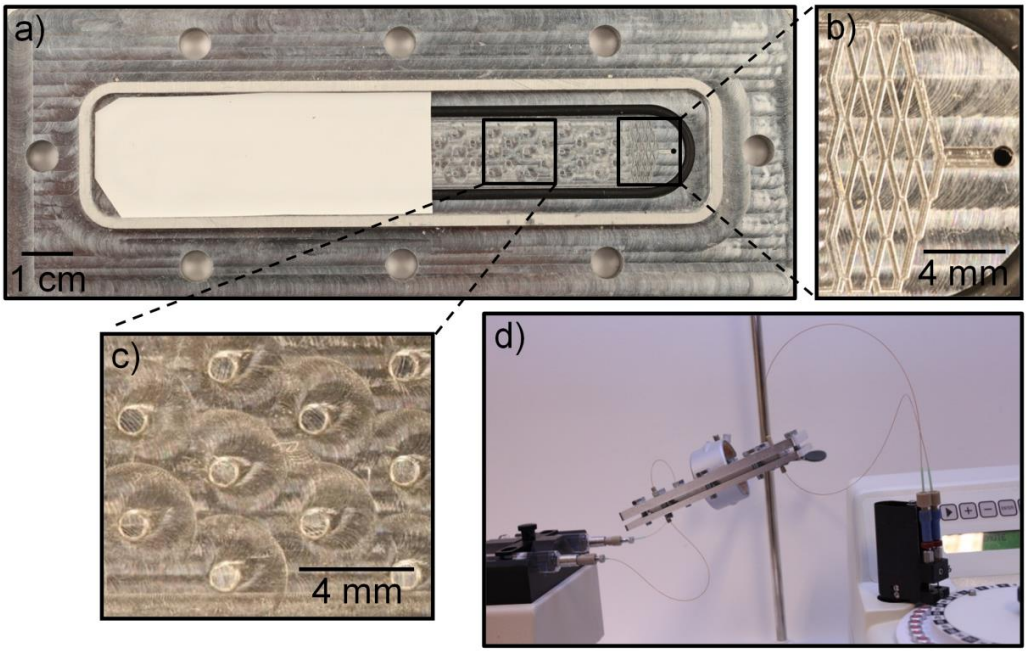

Fig. 1: Representation of the microcontactor a) Overview of the microcontactor b) Distributor to guarantee a uniform flow distribution c) Membrane support pillars to ensure equal spacing (d_{pillar} = 1 mm) d) Microcontactor set-up.

2.3 Numerical simulation

Numerical simulations were performed via a finite difference approach (~10,000 cells), using the Gauss-Seidel iterative algorithm to solve the mass balances in an implicit way. The same case study as in the experiments was simulated i.e., the extraction of 1.3m% 1-propanol out of heptane with pure water. The system operates in steady-state and the boundary walls are two

infinite parallel plates (with an aspect ratio as high as 130), justifying the 2D numerical simulation. The simulations were performed with a PTFE membrane such that the feed solution wets the membrane. Mass transfer inside the feed and extraction solvent channel is described by Eq. 1.

$$u_f \frac{\partial C_f}{\partial x} = D_f \left(\frac{\partial^2 C_f}{\partial x^2} + \frac{\partial^2 C_f}{\partial z^2} \right) \quad (1)$$

$$u_s \frac{\partial C_s}{\partial x} = D_s \left(\frac{\partial^2 C_s}{\partial x^2} + \frac{\partial^2 C_s}{\partial z^2} \right)$$

Since laminar flow conditions apply, the parabolic flow profile is described by the parallel plate Poiseuille expression. Inside the membrane an analogue equation (Eq. 1) is used but with the velocity at zero and an effective diffusion coefficient (Eq 3). Eq. 2 provides the boundary condition at the walls and outlet of the microcontactor.

$$\frac{\partial C}{\partial x} = 0 \quad (2)$$

$$\frac{\partial C}{\partial z} = 0$$

At the inlet of the microcontactor the concentration in the feed side equals to the inlet concentration and in the solvent side the inlet concentration equals zero. At the inlet, a fully developed velocity flow profile is assumed since the channel is preceded by the distributor. At the liquid interface both phases are assumed to be in equilibrium. The simulation was checked via the conservation of mass. Due to time constraints a maximum deviation of 0.16% was allowed.

2.4 Extraction experiments

The feed solution and extraction solvent consisted respectively of 1.3 m% 1-propanol dissolved in heptane and pure water. Pumping of the liquids was performed using one syringe pump (kd Scientific) holding two gastight Hamilton syringes ensuring a fixed feed ratio which was altered using different syringe diameters. Two 10 ml syringes were used for a 1:1 ratio and 25 ml and 10 ml for a 2.5:1 ratio. Samples were cooled while collecting, minimizing solvent loss and analyzed by GC-FID (Agilent, capillary SGE column: 30 m x 0.25 mm, stationary phase: BP21 0.25 µm, 1.3 ml/min He, T_{oven} 110 °C). For each sample the average of 3 GC experiments was determined, with corresponding relative standard deviations of 6%. Collected samples were also controlled for containing only 1 phase to verify that the heptane-water interface was not unstable during the experiment. Before starting a new extraction campaign, a start-up procedure was performed to avoid the presence of air bubbles. This consisted of flushing the microcontactor set-up with methanol for 5 min at a flow rate of 5 ml/min using a HPLC-pump (Shimadzu). A few initial experiments were conducted in a transparent polycarbonate microcontactor to confirm that the flushing procedure was effective in removing the trapped air. The extraction kinetics were measured for different operating conditions (channel depth, flow rate ratio, membrane type, co-current and counter-current) and compared to the derived model for validation.

3. Results

3.1 Flow distributor

When the channel width is much wider than the feed zone, a proper flow distribution at the interface zone is crucial. In the absence of any flow guiding structures the flow profile is severely warped (See Fig. 2a). This would lead to a lower residence time of a liquid segment in the central part of the channel as compared to the zone near the sidewall. As in laminar flow conditions the residence time will determine the extraction efficiency, the flow rate will

be dictated by the residence time of the already further migrated central zone. The sidewall fraction will hence spend more time than necessary and the overall effect would be a lower efficiency compared to when a perfect straight profile would be obtained. In Fig. 2b, the effect of the distributor is demonstrated. Due to the diamond shaped structures radial transport is strongly enhanced with respect to axial transport, resulting in a laterally straight flow profile. These structures can be very easily adapted to much larger ratios of initial and final channel width and can be implemented when conceiving designs for maximizing the flow rates (and hence the channel width).

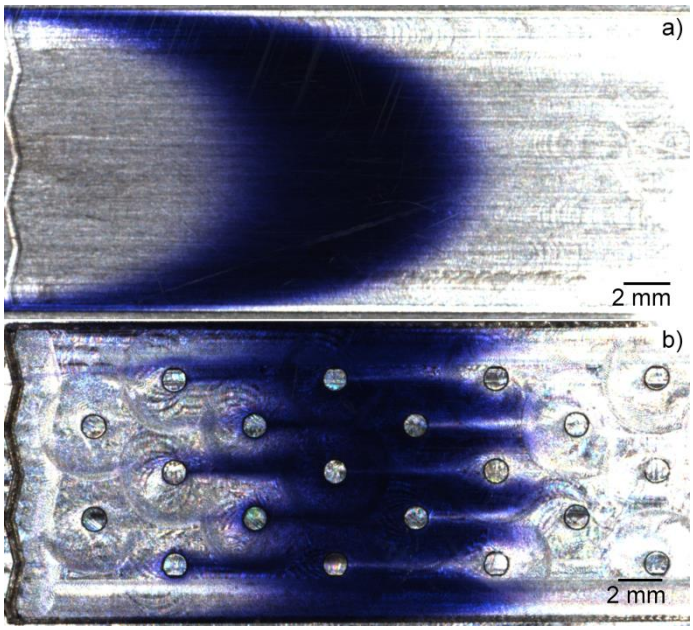

Fig. 2: Injection of a plug of brilliant black BN aqueous solution (V = 2.5 µl, C = 0.022 mg/L) in the microcontactor. a) without distributor, b) with distributor.

3.2 Analytical model

In order to understand the kinetic behavior of the contactor and to allow for optimization a model should be constructed that can be analytically solved with a reasonable degree of accuracy. While kinetic expressions are available in the literature for hollow fibers [2], this is to the best of our knowledge not the case for flat rectangular immiscible liquid-liquid systems. In the constructed model, the following assumptions are taken into account:

- The system operates in steady-state.

- The pores of the membrane are completely wetted by one of the two liquids.
- The partition coefficient is assumed constant.
- Axial diffusion can be neglected (verified by numerical simulation).
- Inside the membrane the effective diffusion coefficient is described by Eq. 3,

$$D_{m,eff} = \frac{\varepsilon D_f}{\tau} \tag{3}$$

where ε is the porosity of the membrane, D is the diffusion coefficient, τ is the tortuosity which was assumed 1 after analysis of SEM-pictures.

Taking these assumptions into account two overall mass transfer coefficients can be found (Fig. 3):

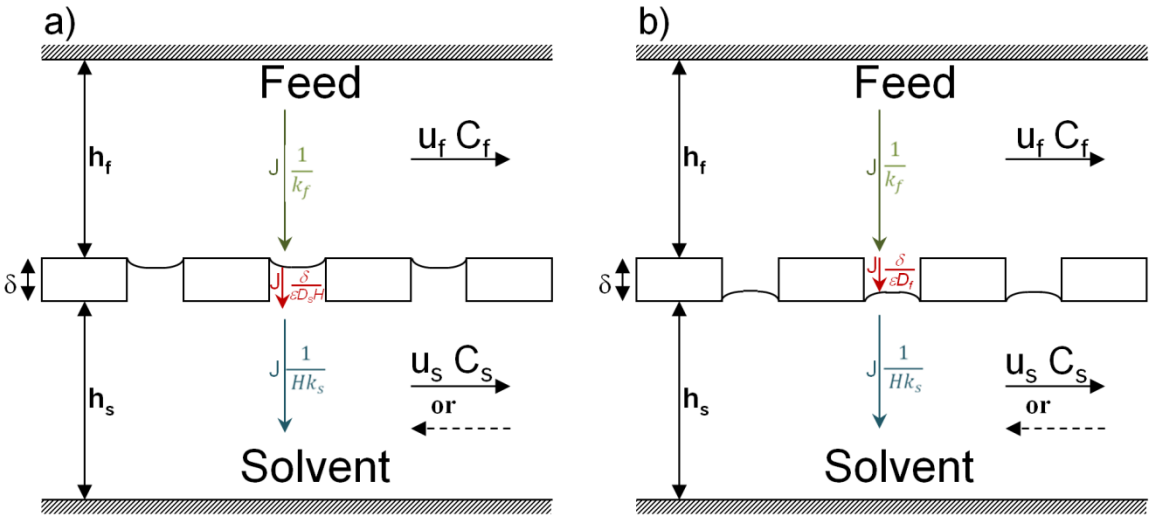

Fig. 3: Schematic representation of the microcontactor with the symbols used throughout the model. a) The extraction solvent wets the membrane, b) The feed phase wets the membrane. h is the channel depth, C is the concentration of the analyte, u is the velocity, δ is the thickness of the membrane, ε is the porosity of the membrane J is the flux, k is the mass transfer coefficient, H is the partition coefficient and the subscript f and s denote respectively the feed and extraction solvent.

(4)

$$1)\ K_s = \frac{1}{\frac{1}{k_f} + \frac{\delta}{D_s \varepsilon H} + \frac{1}{H k_s}}$$

$$2)\ K_f = \frac{1}{\frac{1}{k_f} + \frac{\delta}{D_f \varepsilon} + \frac{1}{H k_s}} \quad (5)$$

where K_s is the overall mass transfer coefficient when the extraction solvent wets the membrane, K_f is the overall mass transfer coefficient when the feed solution wets the membrane, δ is the thickness of the membrane, H is the partition coefficient and k is the mass transfer coefficient. The subscript f and s denotes respectively the feed and extraction solvent. This notation is used consistently throughout the article. The flux from the feed to the extraction solvent equals:

$$J = K(C_f - \frac{C_s}{H}) \quad (6)$$

where J is the flux and C is the concentration of the analyte. From the mass balance written from one side of the membrane a second equation can be derived equalling Eq. 6:

$$-\frac{u_f h_f}{L}\frac{\partial C_f}{\partial x'} = K(C_f - \frac{C_s}{H}) \quad (7)$$

with $x' = \frac{x}{L}$

where u is the velocity, h the depth of the channel, L is the length of the microcontactor and x' is the dimensionless axial length.

3.2.1 Co-current

Out of Eq. 7 the concentration of solute at the outlet of the microcontactor can be derived for co-current with following boundary conditions:

$$x = 0 \rightarrow C_f = C_{f,0} \tag{8}$$

$$x = L \rightarrow C_f = C_{f,L}$$

with subscript 0 and L the location in the microcontactor.

$$C_{f,L} = \frac{C_{f,0} - \frac{C_{s,0}}{H}}{1 + \frac{\alpha_f}{\alpha_s}} e^{-\frac{KL}{u_f h_f}\left(1+\frac{\alpha_f}{\alpha_s}\right)} + \frac{\frac{\alpha_f}{\alpha_s} C_{f,0} + \frac{C_{s,0}}{H}}{1 + \frac{\alpha_f}{\alpha_s}} \tag{9}$$

in which:

$$\alpha_f = \frac{u_f h_f}{KL} \qquad \alpha_s = \frac{u_s h_s H}{KL} \tag{10}$$

In co-current the global mass balance equals:

$$C_{f,L} - C_{f,0} = \frac{\alpha_s}{\alpha_f}\left(\frac{C_{s,0}}{H} - \frac{C_{s,L}}{H}\right) \tag{11}$$

Combining Eqs. 9 and 11 yields an expression that determines the concentration of the solute in the solvent side at the outlet for co-current flow:

(12)

$$C_{s,L} = -\frac{H\alpha_f\left(C_{f,0} - \frac{C_{s,0}}{H}\right)}{\alpha_s + \alpha_f} e^{-\frac{KL}{u_f h_f}\left(1+\frac{\alpha_f}{\alpha_s}\right)} + \frac{H\frac{\alpha_f}{\alpha_s}C_{f,0} + C_{s,0}}{1 + \frac{\alpha_f}{\alpha_s}}$$

The mass transfer coefficient k_f and k_s are generally expressed being contained within the dimensionless Sherwood number (Sh):

$$Sh = \frac{k * 2h}{D} \tag{13}$$

To calculate the Sherwood number two cases can be considered. In the first one the concentration at the membrane is assumed to be constant, which is a realistic approximation when the flow rate of the feed is much higher than the flow rate of the extraction solvent or vice versa. In the second case the flux through the membrane is assumed to be constant. In both cases the opposite wall is assumed impermeable such that there is no flux through this wall. The Sherwood number for both cases can be calculated using the parallel plate Poiseuille expression to approximate the flow profile in flat rectangular channels with high aspect ratios in analogy with the situation of heat transport which is described through the Nusselt number (Nu), with the heat transfer occurring between two plates with an infinitive aspect ratio and with one plate being completely insulating [25]. When a constant membrane concentration is assumed Sh = 4.86, while for constant flux Sh = 5.39 is obtained. Given the similarity of the governing equations, these values are expected to coincide with the Nu numbers obtained for a similar geometry. As the difference between these cases is only 10%, the selected boundary condition has apparently only a small impact on the mass transfer kinetics. Throughout the rest of the paper a constant flux through the membrane is assumed with its corresponding Sh number (see appendix for derivation). This approach can be

considered as a good approximation given the excellent agreement between theoretical and experimental values (see below).

3.2.2 Counter-current

The equation for $C_{f,L}$ and $C_{s,0}$ for counter-current flow can be derived from the global mass balance (Eq. 14) and the mass balances written from one side of the membrane (Eqs. 15 and 16).

$$\frac{C_{s,0}}{H} = \frac{\alpha_f}{\alpha_s}\left(C_{f,0} - C_{f,L}\right) + \frac{C_{s,L}}{H} \tag{14}$$

$$\partial C_f = -\frac{1}{\alpha_f}\left(C_f - \frac{C_s}{H}\right)\partial x \tag{15}$$

$$\partial \frac{C_s}{H} = -\frac{1}{\alpha_s}\left(C_f - \frac{C_s}{H}\right)\partial x' \tag{16}$$

$$\int_{C_{f,0}-\frac{C_{s,0}}{H}}^{C_{f,L}-\frac{C_{s,L}}{H}} \frac{\partial\left(C_f - \frac{C_s}{H}\right)}{C_f - \frac{C_s}{H}} = \frac{1}{\alpha_s} - \frac{1}{\alpha_f}\int_0^1 \partial x \tag{17}$$

$$ln\frac{C_{f,L} - \frac{C_{s,L}}{H}}{C_{f,0} - \frac{C_{s,0}}{H}} = \frac{1}{\alpha_s} - \frac{1}{\alpha_f} \tag{18}$$

Combining Eqs. 14 and 18 produces the relation for $C_{f,L}$ and $C_{s,0}$ for counter-current.

$$C_{f,L} = \frac{C_{f,0}\left(1 - \frac{\alpha_f}{\alpha_s}\right)e^{\left(\frac{1}{\alpha_s} - \frac{1}{\alpha_f}\right)} - \frac{C_{s,L}}{H}e^{\left(\frac{1}{\alpha_s} - \frac{1}{\alpha_f}\right)} + \frac{C_{s,L}}{H}}{1 - \frac{\alpha_f}{\alpha_s}e^{\left(\frac{1}{\alpha_s} - \frac{1}{\alpha_f}\right)}} \tag{19}$$

$$C_{s,0} = C_{s,L} + HC_{f,0}\frac{\alpha_f}{\alpha_s} - \frac{\alpha_f}{\alpha_s}\frac{HC_{f,0}\left(1 - \frac{\alpha_f}{\alpha_s}\right)e^{\left(\frac{1}{\alpha_s} - \frac{1}{\alpha_f}\right)} - C_{s,L}e^{\left(\frac{1}{\alpha_s} - \frac{1}{\alpha_f}\right)} + C_{s,L}}{1 - \frac{\alpha_f}{\alpha_s}e^{\left(\frac{1}{\alpha_s} - \frac{1}{\alpha_f}\right)}} \tag{20}$$

Inspecting Eq. 19 it becomes clear that when $\alpha_f = \alpha_s$ no solution is obtained directly, which can be understood by writing the equation as follows:

$$\lim_{\frac{\alpha_f}{\alpha_s} \to 1} C_{f,L} = \frac{0}{0} \tag{21}$$

Applying l'Hôpital's rule and assuming that $C_{s,L} = 0$, which is in practice correct when the extraction solvent does not contain any analyte initially, the relation for $C_{f,L}$ becomes:

$$C_{f,L} = \frac{\alpha_f}{\alpha_f + 1}C_{f,0} \tag{22}$$

Combining Eqs. 14 and 22 gives the relation for $C_{s,0}$:

(23)

$$C_{s,0} = HC_{f,0}\left(1 - \frac{\alpha_f}{\alpha_f + 1}\right)$$

3.3 Validation of the model

The accuracy of the described model was first evaluated by performing numerical simulations. Next, the influence of the channel depth, the flow rate ratio and the membrane characteristics on to the extraction kinetics were experimentally examined individually and compared with the theoretically expected trends.

3.3.1 Numerical simulation

The kinetic behavior of the extraction was studied for different flow rates. The results are given in Fig. 4 showing that the numerical solution gives a very similar result as the analytically described model (average deviation of 6.9%). The difference between the numerical solution and the analytical model can be attributed in part by the assumption of a constant flux at the membrane in the analytical model and to numerical errors. The system was also solved numerically without the inclusion of the axial diffusion term. This gives an almost identical result (maximal difference below 0.11%) as when taking the axial diffusion term into account. This can be explained by the fact that the convective transport dominates the diffusive transport, justifying the assumption that axial diffusion in the analytical model is negligible.

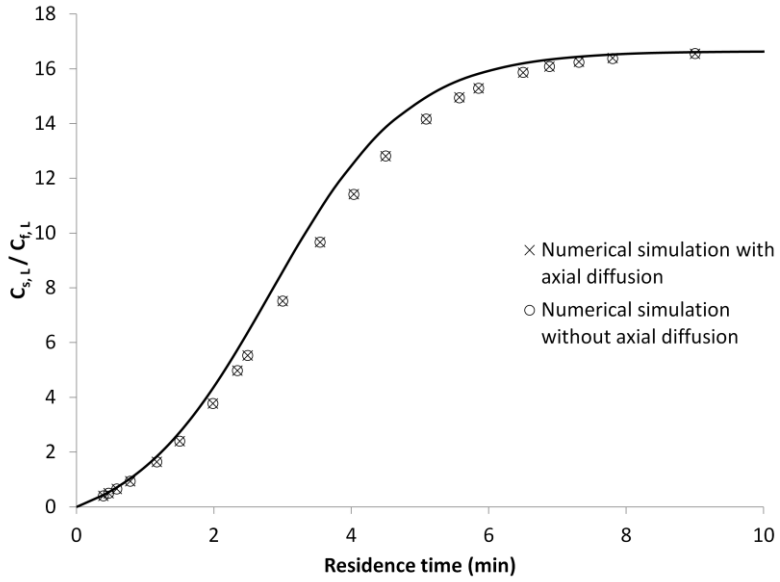

Fig. 4: Numerical simulation of the microcontactor (h = 100 µm, L = 90 mm, w = 13 mm, PTFE-membrane, flow rate ratio 1:1 (feed:extraction solvent), co-flow) extracting 1-propanol out of n-heptane with water. The solid line represents the theoretically expected pattern as predicted by the model.

3.3.2 Experimental study: Co-current

Operating the microcontactor in co-current mode a single extraction stage is obtained in which the equilibrium concentration is eventually reached when sufficient contact time is provided. Increasing the channel depth has a direct impact on the first and last term of the overall mass transfer coefficient (see Eqs. 4 and 5), lowering the contribution of the membrane on the extraction kinetics and slowing it down. Observing Fig. 5 illustrates this phenomenon experimentally as well as the theoretically expected trend. Changing the channel depth of 100µm to 200µm the time to reach equilibrium rises from 9 min to 22 min. This increase can also be intuitively expected as the time needed to diffuse a certain distance scales to this distance with the power of 2. At that moment the concentration ratio ($C_{s,L}/S_{f,L}$) equals the partition coefficient which is 16.6 (determined by a shaking test). In order to draw the model for the extraction of 1-propanol out of heptane the molar diffusion coefficients have to be known. The diffusion coefficient in water was assumed to be 1.05 $x10^{-9}$ m^2/s [26], which is very similar to other published values [27, 28]. For 1-propanol in heptane no literature value

was found and therefore the average value of the best fits in the different described experiments below was used to plot the theoretical curves (2.20 ± 0.67) x10^{-10} m²/s. It should be noted here that this diffusion coefficient was determine with a fitting procedure based on an approximated Sh number assuming constant flux, and that a deviation of the actual Sh number would also influence the diffusion coefficient. To allow for optimization of the microcontactor to given extraction requirements, the use of an (approximate) analytical solution is however crucial and the influence of small deviations of Sh and D_{mol} are of secondary importance in this discussion (see below).

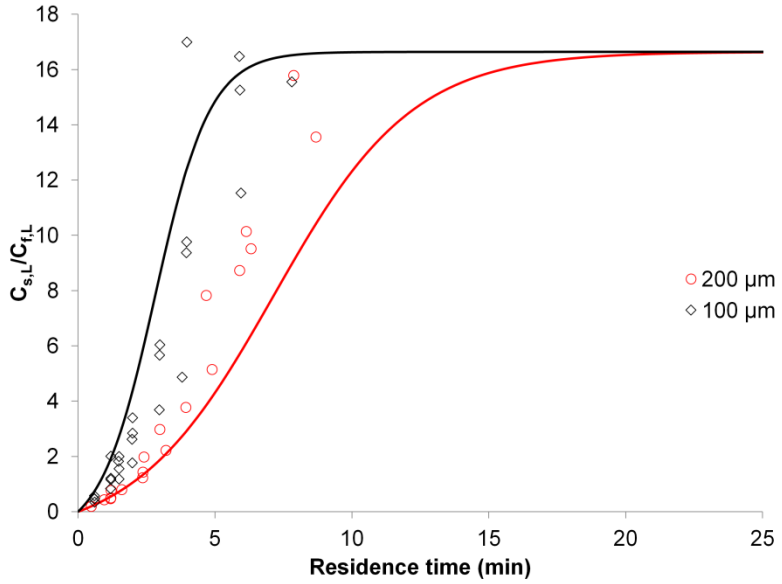

Fig. 5: Extraction kinetics of a microcontactor with a channel depth of 100 or 200µm. Both microcontactors were operated in co-current with the PTFE membrane at a flow rate ratio of 1:1 (feed:extraction solvent). The solid lines represent the theoretically expected pattern as predicted by the model.

Increasing the flow rate of the heptane feed phase appears to enhance the extraction kinetics (Fig. 6). This is expected as the flux is higher because the concentration gradient remains larger throughout the microcontactor compared to the equal flow rate situation. When the solvent flow rate is larger the flux decreases due to a lower concentration gradient. This phenomenon is described by the model and agrees well with the experimentally observed trend. Increasing the flow rate ratio from 1:1 to 2.5:1 (feed:extraction solvent) results in a

residence time of 7.5 min to reach equilibrium instead of 9 min. When the flow rate ratio is the inverse of the viscosity ratio, an identical axial pressure gradient can be achieved, resulting in an equal pressure across the membrane. While no breaktrough was observed below the applied flow rates of up to 200 µl/min for the 100 µm deep reactor, it can be beneficial from a kinetic point of view to reduce the channel height, thereby producing much larger pressure gradients across the membrane when the flow rates are not adapted according to the viscosities. This approach would allow for an unlimited reduction of channel height, with no risk to produce breakthrough of the interphase between the two liquids to the least viscous one (in case of a 1:1 flow rate ratio).

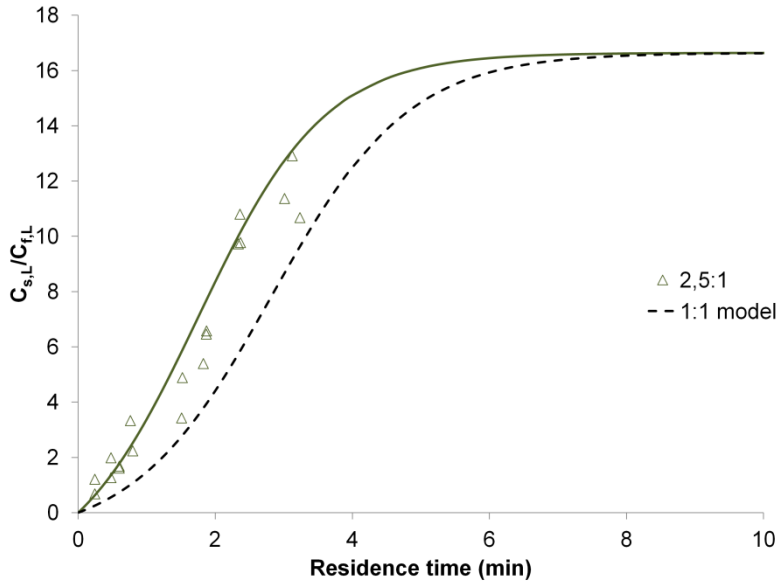

Fig. 6: Extraction kinetics of a 100 µm deep microcontactor operated at a flow rate ratio of 2.5:1 (feed:extraction solvent) in co-current. The microcontactor was equipped with the PTFE membrane. The solid line represents the theoretically expected pattern as predicted by the model.

Changing the Teflon membrane for the polycarbonate membrane (Table 1) the second term of the mass transfer coefficient contributes less to the overall mass transfer resistance because water is now the wetting solvent and consequently the partition coefficient appears in the second term of the nominator of the overall mass transfer coefficient (Eq. 4). With water

filling up the pores it is also the diffusion coefficient of 1-propanol in water that determines the diffusion through the pores and is a factor 4.8 lager than with diffusion in heptane. Using the polycarbonate membrane equilibrium is already reached within 2.1 min in a 100 µm deep microcontactor and a flow rate ratio of 2.5:1 (Fig. 7) With the Teflon membrane a 3.6 times longer residence time is required to reach equilibrium.

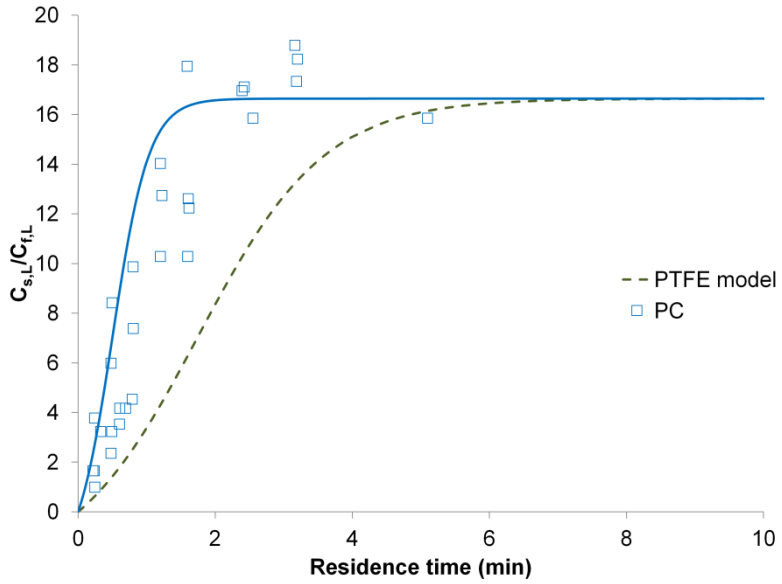

Fig. 7: Extraction kinetic of a 100 µm deep microcontactor operated at a flow rate ratio of 2.5:1 (feed:extraction solvent) equipped with the polycarbonate membrane in co-current. The solid line represent the theoretically expected patterns as predicted by the model.

For both membranes, at least 90 % of the equilibrium is reached in less than 5 min. This creates a vast potential to use the reactor as a screening tool. Some additional extraction time should be provided for systems with lower diffusion and partition coefficient values, and it should also be taking into account that for each combination the contactor should be refilled with the new solution. Generally, it can be assumed that a screening time of 15 min is realistic. This is an extremely interesting feature to find the optimal extraction conditions of a e.g. a pharmaceutical reaction mixture. Often more than 20 combinations are tested by changing the composition of the solvent and feed phase to find a compromise between

maximal extraction of the component of interest and a minimal extraction of side products. By changing the ratios of the flow rates of the feed and the solvent phases, batch extractions with different compositions can be mimicked and the resulting extracts can be collected automatically in a fraction collector (see Fig. 1d for an overview of the automated screening device).

3.3.3 Experimental study: Counter-current

Operating the microcontactor in counter-current mode multiple extraction stages can be obtained, enabling high extraction efficiencies using a single extraction device only. Operating the 200 µm deep microcontactor with a Teflon membrane and a flow rate ratio of 2.5:1, the concentration ratio ($C_{s,0}/C_{f,L}$) reaches the partition coefficient value of 16.6 in 6 min. Performing the same extraction in a 200 µm deep microcontactor in co-current mode requires 19 min according to the model. A huge time gain is hence achieved by performing counter-current operation and by operating at longer residence times the concentration ratio increases even further (Fig. 8).

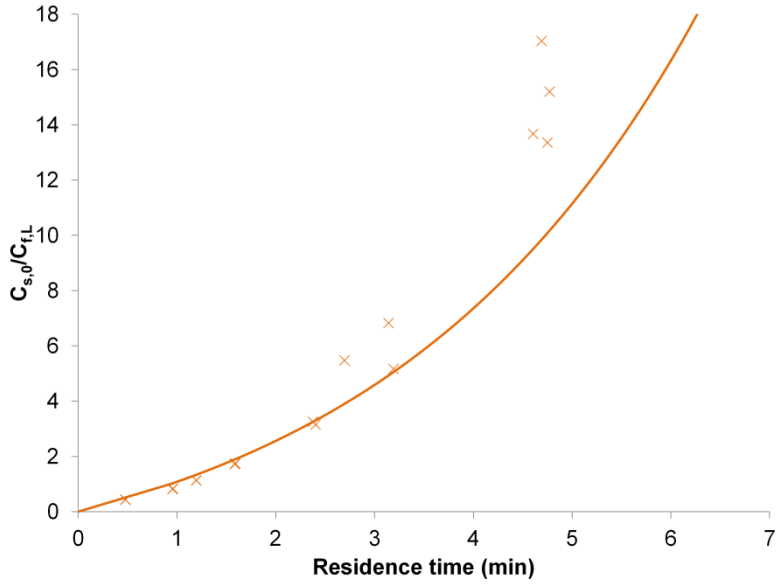

Fig. 8: Extraction kinetic of a 200 µm deep microcontactor operated at a flow rate ratio of 2.5:1 (feed:extraction solvent) equipped with the Teflon membrane in counter-current. The solid line represent the theoretically expected patterns as predicted by the model.

Using the Kremser equation with the assumption that no analyte is initially present in the solvent (Eq. 24) [29], the number of theoretical stages can be calculated (Fig 9a):

$$N = \frac{ln\left(\frac{C_{f,0}}{C_{f,L}}\left(1-\frac{1}{E}\right)+\frac{1}{E}\right)}{ln(E)} \tag{24}$$

$$E = H\frac{Q_s}{Q_f} \tag{25}$$

where N is the number of theoretical stages, E is the extraction factor and Q is the flow rate. Inserting the obtained values in Eq. 24, a value of N = 1 is obtained for a residence time of 6 min. Longer residence times result in concentration ratios above the single stage situation, corresponding to higher numbers of theoretical stages.

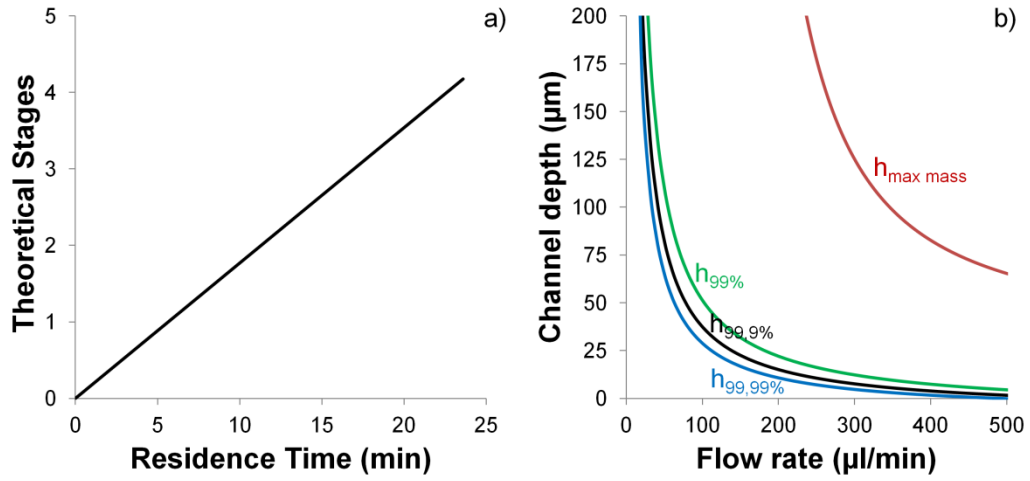

Fig. 9: a) Number of theoretical stages in function of residence time for counter-current extraction (h = 200 µm, Teflon membrane, 2.5:1 (feed: extraction solvent) flow rate ratio), b) Optimal channel depth to obtain a maximal concentration of analyte at the solvent side X = 99% ($h_{99\%}$), X = 99.9% ($h_{99.9\%}$), X = 99.99% ($h_{99.99\%}$) and optimal channel depth for extraction of maximum possible mass of analyte ($h_{max\ mass}$).

Both in co-current as in counter-current mode the theoretical model coincides well with the experimental data. Minor deviations can be caused by measuring errors for instance due to deviations in the GC analysis, the approximated Sh number, the used molecular diffusion coefficients, evaporation of heptane prior to the analysis, an imperfect flat face flow profile and errors in the membrane characteristics given by the manufacturer.

3.4 Optimal channel depth

Operating in co-current mode the channel depth to obtain the maximum concentration of analyte on the solvent side can be calculated out of the proposed model as well as the channel depth for extracting the maximum mass of analyte. The maximum concentration of analyte at the solvent side in co-current is obtained when equilibrium is reached. This is assumed to be the case when $C_{s,L}/C_{f,L}$ equals to a certain fraction (X, e.g.0.999) of the partition coefficient. Dividing Eq. 12 by Eq. 9 and assuming that $C_{s,0}$ equals zero, Eq. 26 is produced:

$$\frac{C_{s,L}}{C_{f,L}} = \frac{1 - e^{-\frac{KL}{u_f h_f}\left(1+\frac{\alpha_f}{\alpha_s}\right)}}{\frac{\alpha_s}{H\alpha_f} e^{-\frac{KL}{u_f h_f}\left(1+\frac{\alpha_f}{\alpha_s}\right)} + \frac{1}{H}} \tag{26}$$

It is assumed that the channel depths, widths and linear velocities in both channels are identical and that a polycarbonate membrane is used, allowing to rewrite Eq. 26 as:

$$\frac{K_s L}{u_f h_f}\left(1+\frac{1}{H}\right) = -ln\frac{1-X}{XH+1} \tag{27}$$

Inserting Eq. 4 into Eq. 27 gives the final equation for the channel depth for maximum concentration ($h_{max\,C}$):

$$h_{max\,C} = \frac{\frac{ShD_f D_s H\varepsilon L\left(1+\frac{1}{H}\right)w}{-Qln\frac{1-X}{XH+1}} - Sh\delta D_f}{\varepsilon H D_s + D_f \varepsilon} \tag{28}$$

where w the width of the microcontactor. Applying this equation to the experimental conditions of the case study, the optimal channel depth in function of the flow rate is obtained (Fig. 9b). This was calculated for 3 different fractions of the partition coefficient at which it is assumed that equilibrium is reached (X = 0.99; 0.999; 0.9999). As flow rates are increased, lower channel depths are necessary due to the reduced residence time in order to reach equilibrium. When a requirement of 99% of the partition coefficient is set, it is obvious that the optimal channel depth is higher. To obtain maximal concentration the highest possible flow rate is 41.6 µl/min for a 100 µm deep (and 13 mm wide) channel, given that at 99.9% of the partition coefficient equilibrium should be reached.

In order to extract the maximum possible mass of analyte the optimal channel depth can be derived as follows, assuming also that the channel depths, velocities and widths in both channels are identical and that a polycarbonate membrane is used. Multiplying Eq. 12 with the flow rate enables to calculate the mass analyte extracted:

(29)

$$C_{s,L}Q = \frac{C_{f,0}uwh}{1+\frac{1}{H}} - \frac{C_{f,0}uwh}{1+\frac{1}{H}}\, e^{-\frac{L\left(1+\frac{1}{H}\right)ShD_sHD_f\varepsilon}{u\left(D_sH\varepsilon h^2+ShD_f\delta h+D_f\varepsilon h^2\right)}}$$

By equalling the derivative from Eq. 29 to zero (Eq. 30), the channel depth that gives the maximum extracted mass of analyte ($h_{max\ mass}$) can be iterative calculated (Eq. 31) in function of the flow rate.

$$\frac{\partial\left(C_{s,L}Q\right)}{\partial h} = 0 \tag{30}$$

$$h_{max\ mass} = -\frac{L\left(1+\frac{1}{H}\right)ShD_sHD_f\varepsilon}{\frac{Q}{wh}\left(D_sH\varepsilon h+ShD_f\delta+D_f\varepsilon h\right)ln\left(\frac{\frac{Q}{wh}\left(h^2D_s^2SH^2\varepsilon Sh+hSh^2D_fD_sH\delta+ShD_fD_sH\varepsilon h^2\right)^2}{\frac{Q}{wh}+hL\left(1+\frac{1}{H}\right)Sh^3D_s^3H^3D_f\varepsilon\left(2D_sH\varepsilon h+ShD_f\delta+2D_f\varepsilon h\right)}\right)} \tag{31}$$

Applying this equation on the same case study it can be seen in Fig. 9b that it is no longer desirable to reach equilibrium to extract as much analyte as possible, this because at a higher flow rate also more analyte enters the microcontactor as the flow rate of the feed and extraction solvent are identical. The optimum thereby does not lie at equilibrium and higher channel depths are obtained.

4. Conclusions

An analytical solution that describes the concentration profile throughout a membrane microcontactor with flat rectangular high aspect ratio channels is presented and numerically and experimentally validated. Critical in using high aspect ratio channels is flow distribution. Using a diamond shaped flow distributor at the front and end of the channel a more laterally

straight flow profile has been produced. Upon optimizing the microcontactor in the near future for handling relative high flow rates the optimal channel depth has been calculated from of the model in order to achieve maximal concentration or maximal mass transfer of analyte at the solvent side.

5. Acknowledgements

W. De Malsche greatly acknowledges the Flemish Fund for Scientific Research (FWO) for support through a Post-Doctoral grant. J. Hereijgers is supported through a specialization grant from the Instituut voor Wetenschap en Technologie (IWT) from the Flanders region.

6. References

[1] E.L. Cussler, Diffusion: Mass Transfer in Fluid Systems, third ed., Cambridge, 2009.

[2] N.A. D'Ella, L. Dahuron, E.L., Cussler, Liquid-Liquid Extractions with Microporous Hollow Fibers, J. Membr. Sci. 29 (1986) 309-319.

[3] F.X. Pierre, I. Souchon, M. Marin, Recovery of sulfur aroma compounds using membrane-based solvent extraction, J. Membr. Sci. 187 (2001) 239-253.

[4] K. F. Jensen, Microreaction engineering - is small better? Chem. Eng. Sci. 56 (2001) 293-303.

[5] J. De Jong, R.G.H Lammertink, M. Wessling, Membranes and Microfluidics: a review, Lab Chip 6 (2006) 1125-1139.

[6] G. Audunsson, Aqueous/aqueous extraction by means of a liquid membrane for sample cleanup and preconcentration of amines in a flow system, Anal. Chem. 58 (1986) 2714-2723.

[7] J.A. Jönsson, L. Mathiasson, Membrane extraction in analytical chemistry, J. Sep. Sci. 24 (2001) 495-507.

[8] M.D. Ramos Payán, H. Jensen, N.J. Petersen, S.H. Hansen, S. Pedersen-Bjergaard, Liquid-phase microextraction in a microfluidic-chip – High enrichment and sample clean-up

from small sample volumes based on three phase extraction, Anal. Chim. Acta. 735 (2012) 46-53.

[9] N.J. Petersen, H. Jensen, S.H. Hansen, S.T. Foss, D. Snakenbog, S. Pedersen-Bjergaard, On-chip electro membrane extraction, Microfluid. Nanofluid. 9 (2010) 881-888.

[10] N.J. Petersen, S.T. Foss, H. Jensen, S.H. Hansen, C. Skonberg, D. Snakenborg, J.P. Kutter, S. Pedersen-Bjergaard, On-Chip Electro Membrane Extraction with Online Ultraviolet and Mass Spectrometric Detection, Anal. Chem. 83 (2011) 44-51.

[11] H. R. Sahoo, J. G. Kralj, K.F. Jensen, Multistep Continuous-flow Microchemical Synthesis Involving Multiple Reactions and Separations, Angew. Chem. Int. Ed. 46 (2007) 5704-5708.

[12] M.N. Kashid, Y.M. Harsche, D.W. Agar, Liquid-Liquid Slug Flow in a Capillary: An Alternative to suspended Drop or Film Contactors, Ind. Eng. Chem. Res. 46 (2007), 8420-8430.

[13] K.P. Nichols, R.R. Pompano, L. Li, A.V. Gelis, R.F. Ismagilov, Toward Mechanistic Understanding of Nuclear Reprocessing Chemistries by Quantifying Lanthanide Solvent Extraction Kinetics via Microfluidics with Constant Interfacial Area and Rapid Mixing, J. Am. Chem. Soc. 133 (2011) 15721-15729.

[14] A.L. Dessimoz, L. Cavin, A. Renken, L. Kiwi-Minsker, Liquid-liquid two-phase flow patterns and mass transfer characteristics in rectangular glass microreactors, Chem. Eng. Sci. 63 (2008) 4035-4044.

[15] T. Maruyama, T. Kaji, T. Ohkawa, K. Sotowa, H. Matsushita, F. Kubota, N. Kamiya, K. Kusakabe, M. Goto, Intermittent partition walls promote solvent extraction of metal ions in a microfluidic device, Analyst. 129 (2004) 1008-1013.

[16] A. Hibara, M. Nonaka, H. Hisamoto, K. Uchiyama, Y. Kikutani, M. Tokeshi, T. Kitamori, Stabilization of Liquid Interface and Control of Two-Phase Confluence and

Separation in Glass Microchips by Utilizing Octadecylsilane Modification of Microchannels, Anal. Chem. 74 (2002), 1724-1728.

[17] M. Tokeshi, T. Minagawa, K. Uchiyama, A. Hibara, K. Sato, H. Hisamoto, T. Kitamori, Continuous-Flow Chemical Processing on a Microchip by Combining Microunit Operations and a Multiphase Flow Network, Anal. Chem. 74 (2002), 1565-1571.

[18] V. Reddy, J.D. Zahn, Interfacial stabilization of organic-aqueous two-phase microflows for a miniaturized DNA extraction module, J. Colloid Interface Sci. 286 (2005) 158-165.

[19] A. Dupuy, V. Athes, J. Schenk, U. Jenelten, I. Souchon, Experimental and theoretical considerations on breakthrough pressure in membrane-based solvent extraction: Focus on citrus essential oil/hydro-alcoholic solvent systems with low interfacial tension, J. Membr. Sci. 378 (2011) 203-213.

[20] Z.X. Cai, Q. Fang, H.W. Chen, Z.L. Fang, A microfluidic chip based liquid-liquid extraction system with microporous membrane, Anal. Chim. Acta. 556 (2006) 151-156.

[21] J. Hereijgers, M. Callewaert, T. Breugelmans, H. Ottevaere, D. Cabooter, W. De Malsche, A membrane microcontactor as a tool for integrated sample preparation, J. Sep. Sci. 35 (2012), 2407-2413.

[22] J. Vangelooven, W. De Malsche, J. Op De Beeck, J. Eghbali, H. Gardeniers, G. Desmet, Design and evaluation of flow distributors for microfabricated pillar array columns, Lab Chip 10 (2010), 349-356.

[23] A. Berthod . M. Hassoun . M. J. Ruiz-Angel, Alkane effect in the Arizona liquid systems used in countercurrent chromatography, Anal. Bioanal. Chem. 383 (2005) 327–340

[24] K. Farhadi, M. Hatami, A.A. Matin, Microextraction techniques in therapeutic drug monitoring, Biomed. Chromatogr. 26 (2012) 972-989.

[25] P.A. McCuen, W.M. Kays, W.C. Reynolds, Heat Transfer with Laminar and Turbulent Flow Between Parallel Planes with Constant and Variable Wall Temperature and Heat Flux, California, 1962.

[26] H.A. Kooijman, A Modification of the Stokes-Einstein Equation for Diffusivities in Dilute Binary Mixtures, Ind. Eng. Chem. Res. 41 (2002) 3326-3328.

[27] L. Hao, D.G. Leaist, Binary Mutual Diffusion Coefficients of Aqueous Alcohols Methanol to 1-Heptanol, J. Chem. Eng. Data 41 (1996) 210-213.

[28] C.L. Yaws, Transport Properties of Chemicals and Hydrocarbons, first ed., New York, 2009.

[29] R.H. Perry, D.W. Green, Chemical Engineers' Handbook, seventh ed., New York, 1999.

Apendix

Sh for constant flux through the membrane

The flux in the channel equals to:

$$J = -D\frac{\partial C}{\partial z} = -k(C_{mean} - C_{membrane}) \tag{A.1}$$

$$u\frac{\partial C}{\partial x} = D\frac{\partial^2 C}{\partial z^2} \tag{A.2}$$

where C_{mean} is the concentration of the analyte averaged out over the channel height, $C_{membrane}$ is the concentration of the analyte at the membrane, z is the lateral length. The parallel plate Poiseuille expression to approximate the flow profile in flat rectangular channels with high aspect ratios equals to:

$$u = \frac{\Delta p}{2\eta L}(h - z)z \tag{A.3}$$

where Δp is the pressure drop, η is the dynamic viscosity. The velocity is maximal at $z = \frac{h}{2}$:

$$u = \frac{4\,u_{max}}{h^2}(h - z)z \tag{A.4}$$

The boundary conditions are:

$$z = h \qquad \frac{\partial c}{\partial z} = 0 \tag{A.5}$$

$$z = 0 \qquad C = C_{membrane}$$

Combining Eqs. A.2 and A.4 Eq. A.6 is derived taking the boundary conditions in to account and the fact that the flux trough the membrane is constant and no flux through the opposite wall is possible. This implies that $\frac{\partial C}{\partial x} =$ constant.

$$C - C_{membrane} = \frac{2\,u_{max}}{D\,h^2}\frac{\partial C}{\partial x}\left(\frac{h\,z^3}{3} - \frac{z^4}{6} - \frac{h^3\,z}{3}\right) \tag{A.6}$$

The average concentration in the channel can be calculated as follow:

$$C_{mean} - C_{membrane} = \frac{1}{h\, u_{mean}} \int_0^h (C - C_{membrane}) u \partial z \tag{A.7}$$

The average velocity equals to 2/3 of the maximum velocity in the parallel plate geometry:

$$u_{mean} = \frac{2}{3} u_{max} \tag{A.8}$$

Combining Eqs. A.6-A.8 gives:

$$C_{mean} - C_{membrane} = -\frac{26}{105} \frac{u_{max}}{D} h^2 \frac{\partial C}{\partial x} \tag{A.9}$$

$\frac{\partial C}{\partial z}$ at the membrane (z = 0) can be derived out of Eqs. A.2 and A.4 taking the boundary conditions in to account:

$$\frac{\partial C}{\partial z}(z = 0) = \frac{2\, u_{max}}{3\, D} h \frac{\partial C}{\partial x} \tag{A.10}$$

Combining Eqs A.1, A.9 and A.10 gives:

$$\frac{k\, h}{D} = 2.69 \tag{A.11}$$

The Sh number (Eq. 13) for flow between parallel plates with an infinite aspect ratio and a constant flux through the membrane and no flux through the opposite wall hence equals:

$$Sh = 5.38 \tag{A.12}$$

This number is identical as the Nusselt number in heat transfer [25].